Journal of Physics and Chemistry of Solids 72 (2011) 341–346

Contents lists available at ScienceDirect

Journal of Physics and Chemistry of Solids

journal homepage: www.elsevier.com/locate/jpcs

Interplay of matrix element, self-energy and geometric effects in various spectroscopies of the cuprates

A. Bansil [a,*], Susmita Basak [a], Tanmoy Das [a], Hsin Lin [a], M. Lindroos [a,b], J. Nieminen [a,b], Ilpo Suominen [b], R.S. Markiewicz [a]

[a] Physics Department, Northeastern University, Boston, MA 02115, USA
[b] Institute of Physics, Tampere University of Technology, P.O. Box 692, 33101 Tampere, Finland

ARTICLE INFO

Available online 7 October 2010

Keywords:
C. *Ab initio* calculations
C. Neutron scattering
C. Photoelectron spectroscopy
C. STM
D. Optical properties

ABSTRACT

We discuss a comprehensive scheme for modeling various highly resolved spectroscopies of the cuprates where effects of matrix element, crystal structure, strong electron correlations, and superconductivity are included realistically in material-specific detail. A number of illustrative examples drawn from our recent work are presented. Specific issues in the cuprate physics considered are: (i) Origin of high-energy kink or the waterfall effect; (ii) Dichroic effects in angle-resolved photoemission spectrum; (iii) Asymmetry of the scanning tunneling spectrum between the processes of electron extraction and injection; (iv) Persistence of 'Mott' like high-energy features with doping in optical spectra; (v) Magnetic excitations in electron and hole doped cuprates.

1. Introduction

Spectroscopies resolved highly in momentum, energy and/or spatial dimensions are playing an increasing role in unraveling key properties of wide classes of novel materials. However, spectroscopies do not usually provide a direct map of the underlying electronic spectrum, but act as a complex 'filter' to produce a 'mapping' of the underlying energy levels, Fermi surfaces (FSs) and excitation spectra. We may refer to the connection between the electronic spectrum and the measured spectra as a generalized 'matrix element effect' [1]. The nature of the matrix element involved differs greatly between different spectroscopies. For example, in scanning tunneling microscopy/spectroscopy (STM/STS), a sharp tip placed close to the surface of the solid measures the tunneling current in real space. This is very different from what happens in K-edge resonant inelastic X-ray scattering (RIXS), where an X-ray photon is scattered after inducing electronic transitions near the Fermi energy through an indirect second order process, or in angle-resolved photoemission (ARPES) where an incoming photon knocks out an electron from the material. For any given spectroscopy, the matrix element is, in general, a complex function of the phase space of the experiment, e.g. energy/polarization of the incoming photon and the energy/momentum/spin of the photoemitted electron in the case of ARPES. The matrix element can enhance or suppress signals from specific states, or merge signals of groups of states, making a good understanding of the matrix element effects important for not only a robust interpretation of the spectra, but also for ascertaining optimal regions of the experimental phase space for zooming in on states of the greatest interest.

Turning to the cuprates, in order to obtain a realistic description of various spectroscopies, we must include not only the effects of the matrix elements and the complexity of the crystal structure, but also of strong electronic correlations beyond the local density approximation (LDA)-based conventional picture, so that the physics of kinks, pseudogaps and superconductivity can be taken into account properly. In this connection, we have developed a self-consistent, intermediate coupling scheme informed by material-specific, first-principles band structures, where electron correlation effects beyond the LDA are incorporated via appropriate self-energy corrections to the electron and hole one-particle Green's functions [2–6]. Superconductivity is treated by introducing a d-wave pairing term in the Hamiltonian, and antiferromagnetic (AFM) order is used as the simplest model of a competing order. A number of salient features of the resulting electronic spectrum and its energy, momentum and doping dependencies are in accord with experimental observations in electron as well as hole doped cuprates. Our scheme thus provides a reasonable basis for undertaking a comprehensive, beyond-LDA level of modeling of various spectroscopies.

The applications discussed in this article are concerned with a number of issues of current interest to the high-T_c community. The specific topics considered are: (i) Origin of the high-energy

* Corresponding author.
E-mail address: bansil@neu.edu (A. Bansil).

0022-3697/$ - see front matter © 2010 Elsevier Ltd. All rights reserved.
doi:10.1016/j.jpcs.2010.10.003

kink (HEK) or the waterfall effect: By carrying out computation of the ARPES spectrum in $Bi_2Sr_2CaCu_2O_8$ (Bi2212) where effects of the matrix element and the self-energy corrections are included, we show that the HEK is a genuine signature of electronic excitations; (ii) Dichroic effects in ARPES spectrum: We have computed the dichroic effect in Bi2212 for the known high- and low-temperature orthorhombic crystal structures using left- and right-handed circularly polarized light to reveal the sensitivity of dichroic effects to structural details. The observed dichroic effects can be understood essentially within the conventional picture without the need to invoke time-reversal symmetry breaking scenarios; (iii) Asymmetry of the STS spectrum for electron extraction and injection: We model the STS spectrum in Bi2212 realistically by including all relevant orbitals in the system, and compute the tunneling current directly from the semi-infinite solid surface. Our weak coupling computations reproduce the experimentally observed asymmetry due to the opening of new tunneling channels with increasing negative bias voltage; (iv) Persistence of 'Mott' like high-energy features with doping in optical spectra: In accord with experiments, our optical spectra computed within the RPA show that high-energy Mott-like features in NCCO and LSCO persist over the entire doping range including the overdoped system; (v) Magnetic excitations in cuprates: A computation of the magnetic structure factor within our comprehensive model is found to reproduce many of the characteristic features observed in neutron scattering experiments in electron as well as hole doped cuprates.

Within space limitations, this article gives an overview of our results related to the issues in cuprate physics outlined in the preceding paragraph. Much of this work has been or will be presented in greater detail elsewhere. It is hoped nevertheless that the present article, which pulls together some of our recent work on a number of different spectroscopies, will provide a useful overview.

2. Description of the model: Incorporating self-energy corrections, pseudogap physics and superconductivity

Our basic strategy is to add appropriate self-energy terms to the 'uncorrelated' Hamiltonian. This approach is well-suited for our purposes because our modeling of various spectroscopies at its core involves an electron or a hole one-particle Green's function. We now describe briefly a specific self-energy model which seems to provide a tangible starting point for unfolding self-energy effects in the cuprates at a fairly sophisticated level. We illustrate our scheme by considering the case of a one-band Hubbard model, and return to comment on various generalizations below. The Hamiltonian is

$$H=\sum_{k,\sigma}[\epsilon_k c^{\dagger}_{k,\sigma}c_{k,\sigma}+(\Delta_k c^{\dagger}_{k,\sigma}c^{\dagger}_{-k,-\sigma}+c.c.)+US(c^{\dagger}_{k+Q_{AF},\sigma}c_{k,\sigma}+c.c.)], \quad (1)$$

Here, much of the notation is standard. In particular,

$$\Delta_k=\frac{\Delta}{2}[\cos k_x a-\cos k_y a], \quad (2)$$

gives the d-wave superconducting gap through its momentum dependence. Here, a is the in-plane lattice constant, $Q_{AF}=(\pi,\pi)$, U is the Hubbard on-site repulsion and S denotes staggered magnetization, so that the US term introduces AFM order as a simple model of the pseudogap as a competing order. We then evaluate the self-energy through a GW type self-consistent scheme as a function of doping. In general, the self-energy and various Green's functions now are 4×4 tensors. The self-energy for the paramagnetic case is a simple scalar given by [5]

$$\Sigma(k,\omega)=\frac{1}{2}U^2\sum_q\int\frac{d\omega'}{2\pi}G(k+q,\omega+\omega')\Gamma\chi''(q,\omega), \quad (3)$$

where χ is the RPA susceptibility, and a vertex correction Γ is included. We emphasize a number of points in this connection: (i) The self-energy based on Eqs. (1)–(3) involves essentially only one free parameter, which is the value of the Hubbard U for the half-filled case. Effective U values at different dopings are obtained via a self-consistent procedure [5]. The uncorrelated material-specific band dispersion ϵ_k is obtained from first-principles band theory computations [7]. The doping dependence of band parameters is neglected in the spirit of a rigid band model. This is a reasonable approximation in cuprates for doping away from the cuprate planes. However, for doping within the cuprate planes (e.g. replacing Cu by Ni or Zn) or in the pnictides, more sophisticated treatment of disorder effects will be needed [8–10]. (ii) Although the pairing potential could, in principle, be computed from magnetic fluctuations [11,12], for simplicity, we take it as a parameter to reproduce the experimentally measured superconducting gap as a function of doping; (iii) The AFM order as a model of the competing order invoked above is a reasonable choice for electron-doped cuprates [13,14], but it seems also to capture some of the key physics of hole doped cuprates [15], especially when this physics is dominated by the symmetry of the order [16]; (iv) We can in principle include a self-energy for electron–phonon coupling by replacing $U^2\chi''$ in Eq. (3) by α^2F, the Eliashberg function, although the importance of electron–phonon interaction in the cuprates remains controversial [17–19]; (v) The preceding discussion has been cast in terms of a single orbital, but the generalization to treat multiple orbitals is straightforward. This is needed obviously for pnictides where several orbitals are involved at the Fermi energy. Furthermore, in the case of multiple orbitals, more complex superconducting order parameters than the simple d-wave form of Eq. (2) are needed.

In actual computations of spectra for various spectroscopies, we add the preceding tight-binding-based self-energy corrections into the first-principles framework as far as possible. This is straightforward for the cuprates where the physics of correlations is dominated by a single effective orbital and correlation effects on other orbitals and final states are less important. Nevertheless, our scheme thus is not a purely first-principles scheme, but for making progress in treating superconductivity, kinks, nano-scale phases and other effects in complex materials, it will be difficult to make headway on a totally first-principles basis in the near future, and judiciously constructed hybrid schemes of the sort outlined above are unavoidable.

Notably, we have shown that the self-energy based on Eqs. (1)–(3) is in reasonable accord with the limited available QMC results [6,20] and that this self-energy captures a number of key features of the electronic spectra of the cuprates remarkably well. In particular, in accord with experimental observations: Ref. [5] shows how a residual Mott gap feature can persist in the optical spectrum well into the overdoped regime, even after the pseudogap has collapsed; Ref. [14] explains how a change of the Fermi surface topology can make the penetration depth appear to be consistent with s-wave in the strongly underdoped electron-doped cuprates; and, Ref. [6] shows how the dispersion and spectral weight renormalization factors can differ greatly in underdoped cuprates.

3. Origin of high-energy kink in the ARPES spectrum of Bi2212

Fig. 1(a) of the ARPES spectrum taken at 81 eV photon energy from an overdoped sample of Bi2212 shows the high-energy kink

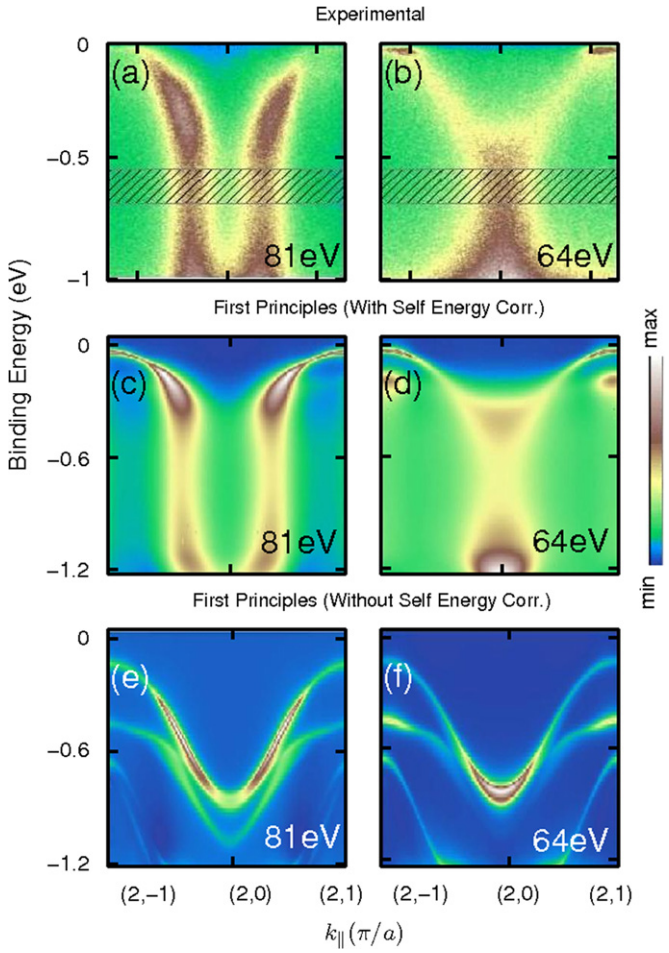

Fig. 1. (Color online) Experimental ARPES spectra [21] from Bi2212 at 81 and 64 eV photon energies in panels (a) and (b), respectively, are compared with the corresponding theoretical spectra based on first-principles one-step computations. In panels (c) and (d), self-energy corrections are included in the computations, while in panels (e) and (f) these corrections are excluded. The weak third band at high binding energies in panels (e) and (f) is a band that moves closer to the Fermi energy in the absence of self-energy corrections, and is not seen in panels (c) and (d). (After Ref. [28].)

(HEK) in dispersion in the 0–1 eV energy range [21]. This effect is also often referred to as the 'waterfall effect' because the spectrum in Fig. 1(a) looks like a pair of waterfalls [22–25]. HEKs in the cuprates have been interpreted as providing evidence for the presence of a high-energy bosonic mode, which could provide a viable electronic mechanism of high-temperature superconductivity [12,26,27]. Fig. 1(b), however, shows that the same sample yields a very different looking spectrum when the measurement is carried out at a different photon energy of 64 eV. At 81 eV in Fig. 1(a), the intensity is low in the momentum region between the two waterfall features, but in sharp contrast, at 64 eV in Fig. 1(b), the spectrum possesses a 'Y-shape' with two arms of the Y connecting a region of high intensity. These results lead naturally to the speculation that the HEK may be an artifact produced by the nature of the photoemission process, i.e. effects of the ARPES matrix element, and that it is not reflective of a bosonic mode of the electronic system [21].

In this connection, Figs. 1(c) and (d) give our computed first-principles ARPES spectra at 81 and 64 eV, respectively [28]. Here, effects of electronic correlations beyond the LDA picture are incorporated in the computations via self-energy corrections along the lines of Section 2 above, in addition to those of the ARPES matrix element [29]. Theoretical spectra are seen to clearly reproduce the remarkable change from waterfall to the Y-shape at different photon energies observed experimentally. In order to highlight the role of self-energy corrections, panels (e) and (f) show the corresponding computed spectra where matrix element effect is included, but the self-energy corrections are turned off in the computations. Results now bear little resemblance to the measured spectra, and do not display the characteristic waterfall or Y-shape at either photon energy. In particular, the ARPES matrix element alone cannot yield the waterfall effect. Results of Fig. 1 demonstrate clearly that the HEK or the waterfall effect in the cuprates is a genuine signature of strong coupling of quasiparticles to electronic excitations, even though the ARPES matrix element plays a substantial role in shaping the spectra.

4. Dichroic effects in the ARPES spectra of Bi2212

It has been suggested that dichroic effects in ARPES spectra using circularly polarized light could be used to test the time-reversal symmetry breaking associated with circulating current scenarios that have been proposed for the pseudogap phase of the cuprates [30]. Specifically, the observation of a non-zero dichroic signal from a high symmetry plane [31] would provide evidence in support of circulating currents. In this connection, we have carried out realistic first-principles ARPES computations [32] to assess the importance of geometric effects, i.e. effects of complexity of the lattice structure, on dichroism in cuprates with the example of Bi2212. Results of Fig. 2 highlight how a finite dichroic signal is indeed obtained when orthorhombic distortions are included in the modeling of ARPES spectra. The left-handed (LH) circularly polarized light now gives the spectrum in Fig. 2(a), which differs from that for right-handed (RH) polarized light in Fig. 2(b), resulting in the dichroism shown in panel 2(c).

More quantitatively, using the known high-temperature (HT) and low-temperature (LT) bulk crystal structures of Bi2212, [33] we found that the orthorhombic distortion in the Bi–O plane in going from the HT to the LT structure induces an increase in the dichroic signal of 1.5%–3.5% (depending on photon energy), which is comparable to the dichroic effect of 3% reported in thin-film measurements of Ref. [31] in the pseudogap phase. Moreover, our computed dichroic signal of 6% at 49.7 eV photon energy for the HT structure is comparable to the 5% effect reported on single crystals [34]. We emphasize that a 1% dichroic effect can be induced by an in-plane movement of O-atoms in the BiO layer by

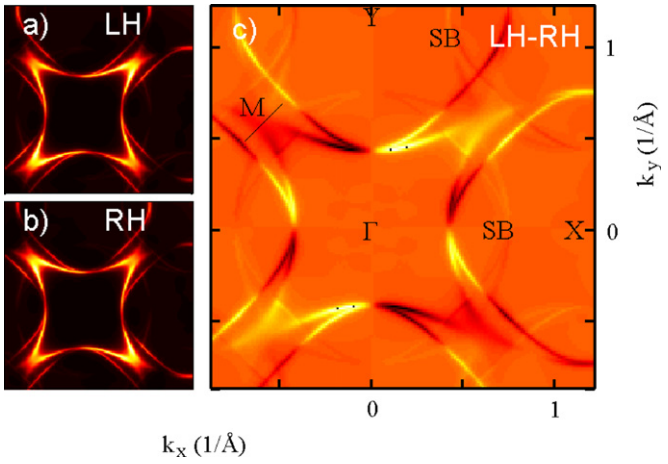

Fig. 2. (Color online) First-principles computation of ARPES spectrum from orthorhombic Bi2212 for left-handed (LH) and right-handed (RH) circularly polarized light showing dichroism resulting from geometric effects in panel (c) within the conventional picture. (After Ref. [32].)

only 0.03 Å, which is well below the accuracy with which lateral positions of surface atoms can be determined currently via surface sensitive probes. Also, in the presence of twinning, our simulations show that a 1% dichroic effect can result from only a 4% change in the population of one of the twins.

In this way, we have clearly established the sensitivity of dichroism to structural details and the viability of the geometric mechanism in explaining existing measurements, and demonstrated that the detection of time reversal symmetry breaking via ARPES will be complicated by the masking effects of lattice distortions. In interpreting observed dichroic effects and their temperature/doping dependencies, we should keep in mind the possibility of variation in geometrical and domain structure as a function of temperature and/or doping, especially in the surface region due to the surface-sensitivity of ARPES. Results of Fig. 2 provide an example of how a careful assessment of factors involved in a conventional view of cuprate physics can inform the search for exotic phases.

5. High-energy asymmetry of the STM spectrum of Bi2212

Much of the existing interpretation of the STS spectra from the cuprates is based on the assumption that the spectrum is directly proportional to the local density of states (LDOS) of the anti-bonding band obtained by hybridization of the Cu-$d_{x^2-y^2}$ with O-$p_{x,y}$ orbitals. This view of STS neglects effects of the tunneling process in modifying the spectrum in the presence of the insulating overlayers. In order to assess the effects of the tunneling matrix element, we have carried out realistic modeling of the STS spectrum in Bi2212, where all relevant orbitals are included and the tunneling current to the tip placed on the semi-infinite solid surface is computed directly [35]. Fig. 3(a) compares the calculated and measured [36] STS spectrum in overdoped Bi2212 with the LDOS of the anti-bonding band. At high positive bias voltages, the computed spectrum (black line) is quite structureless, but at low energies, a gap with the characteristic peak-dip-hump features can be seen. The computed spectrum displays the presence of bonding and anti-bonding van Hove singularities (VHSs) as two distinct peaks, followed by a broad dip around -0.7 eV and a subsequent increase in intensity. The aforementioned features of the theoretical spectrum are in substantial accord with the experimental results (red line). Most notably, theory reproduces the pronounced experimentally observed asymmetry of the tunneling spectrum between positive and negative biases. The rapid increase in current at high negative bias results from increasing spectral weight of Cu d_{z^2} and other orbitals which contribute to the 'spaghetti' of bands starting around 1 eV binding energy in Bi2212. It is clear that the LDOS of the Cu $d_{x^2-y^2}$ band given by the green line in Fig. 3(a) does not provide a good description of the spectrum, and that the LDOS in fact possesses an asymmetry which is opposite to that of the tunneling spectrum.

Fig. 3(b) shows the computed 'topographic map' of the BiO surface in constant current mode. Bi atoms appear as bright spots in accord with experimental observations, while O atoms sit at the centers of dark regions. An analysis of the theoretical STS spectrum in terms of various tunneling channels or paths to the tip shows that the $d_{x^2-y^2}$ orbital of the Cu atom lying right under the Bi atom gives zero contribution to the current. The dominant contribution to the spectrum comes from the four nearest neighbor Cu atoms as depicted schematically in Fig. 3(c), in accord with the conclusions of Ref. [37].

Results of Fig. 3 establish clearly that effects of the tunneling matrix element in the cuprates are very substantial, and that the STS spectrum is modified greatly from the LDOS of the Cu-$d_{x^2-y^2}$ orbital. Moreover, the striking asymmetry of the STS spectrum in Bi2212 can be understood naturally within the conventional picture, indicating that effects of strong correlations are more subtle than thought previously [38]. Our scheme can be extended straightforwardly to incorporate effects of self-energy corrections, and to treat impurities and nano-scale inhomogeneities.

6. Persistence of Mott physics in the optical spectra of cuprates

Optical spectra in electron and hole doped cuprates were measured quite early [39], but still harbor significant puzzles and offer remarkable insight into the nature of electronic states in the

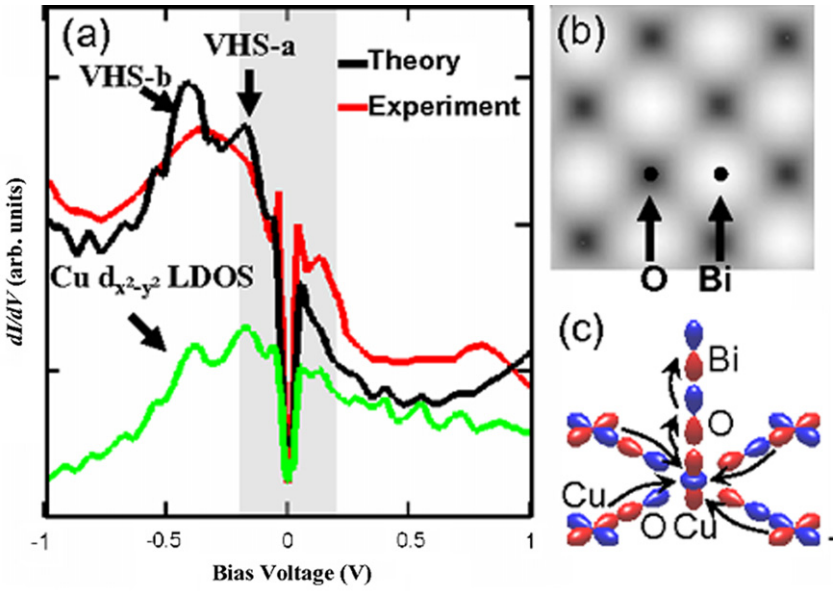

Fig. 3. (a) Computed STS signal in Bi2212 (black line) within the conventional picture shows the characteristic anisotropy between positive and negative bias voltage seen in experiment (red line) [36]. Green line gives the LDOS of the Cu-$d(x^2-y^2)$ orbital. (b) Topographic map. (c) Main tunneling channel to surface Bi atoms. (After Ref. [35].) (For interpretation of the references to colour in this figure legend, the reader is referred to the web version of this article.)

cuprates. This can be seen by reference to the experimental data points for NCCO in Fig. 4(a), although the following commentary is also applicable to the case of LSCO in Fig. 4(b). The half-filled insulator displays the expected Mott gap with intensity rapidly decreasing below 1.5 eV. As the insulator is doped, spectral weight shifts rapidly from the high-energy Mott feature around ~ 1.7 eV to a new mid-infrared (MIR) peak around 0.5 eV and the Drude peak near $\omega = 0$. But even in the overdoped case, where the MIR peak has collapsed, there is spectral weight at high energies. This persistence of Mott-like feature into the overdoped regime is a telltale signature that weak coupling physics embodied in the LDA is fundamentally unable to capture some key aspects of electronic states in the cuprates and that 'beyond LDA' schemes must be deployed. Accordingly, we have carried out calculations of optical conductivity within the one-band model in LSCO and NCCO over the full doping range within the RPA framework [5]. Effects of GW-type self-energy corrections discussed in Section 2 above are included in these computations, along with those of a (π,π) AFM order as a model of the competing order. Fig. 4 shows that our theory reproduces the doping dependencies of the experimental spectra in substantial detail, including the rapid shift of spectral weight from high to low and intermediate energies, and persistence of Mott-like features at high energies.

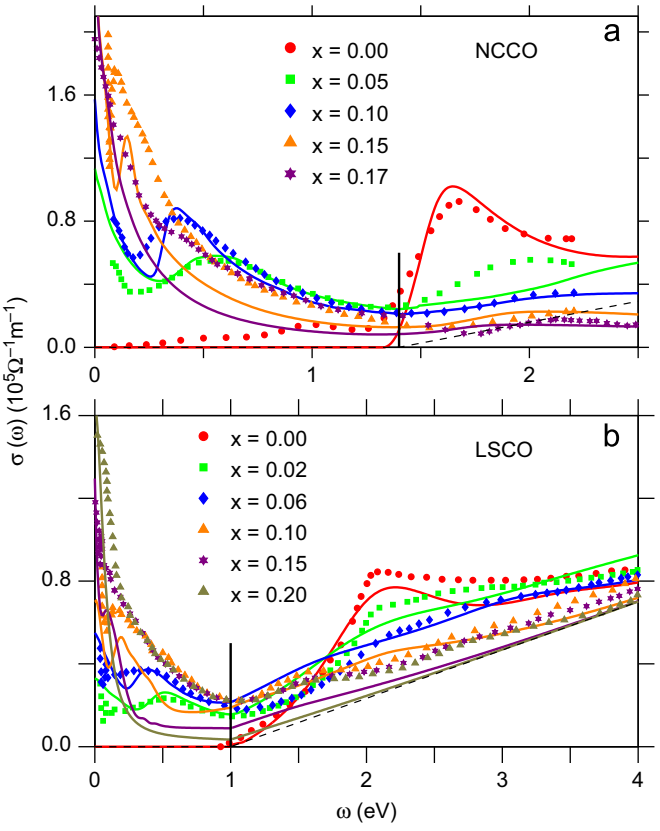

Fig. 4. (Color online) Computed optical spectra in LSCO and NCCO as a function of doping are compared with the corresponding experimental results [39] as discussed in the text. (After Ref. [5].)

Our analysis of the theoretical spectra of Fig. 4 reveals that the rapid loss of high-energy spectral weight, and the associated shift of the MIR feature to lower energies with doping reflects collapse of the pseudogap order due to the presence of a quantum critical point near optimal doping in the coherent in-gap states. This is seen also in RIXS and ARPES studies [13,40]. In sharp contrast, the gap in the incoherent states persists at all dopings, including the overdoped regime. The coherent and incoherent states are connected via a high-energy kink (discussed also in Section 3 above in connection with ARPES spectra), which is driven mainly by magnetic excitations.

7. Magnetic excitations in cuprates

Neutron scattering has revealed the presence of the so-called magnetic resonance peak in the magnetic excitation spectra of cuprates [41]. The existence of this mode has also been confirmed via various other spectroscopies. This low-energy mode is approximately commensurate at (π,π), and its dispersion exhibits considerable material dependence. The intensity is found to scale with the order parameter in all cuprates [42], suggesting an intimate connection with the mechanism of high-T_c. Despite many theoretical proposals in the literature [43], the nature and origin of this resonance and its possible relationship to low-energy kinks seen in ARPES remain a matter of controversy.

In this connection, Fig. 5 shows the computed magnetic excitation spectra, which we have obtained in the superconducting state in optimally doped LSCO and PLCCO by computing RPA-based magnetic susceptibility in the one-band model [44]. Here, as in the case of optical spectra discussed in Section 6 above, self-energy corrections within our GW framework have been included. The superconducting gap parameter has been adjusted to match the experimentally observed gap values. No other adjustable parameters have been invoked in the modeling. Theoretical spectra in Fig. 5 are seen to reproduce the key features of the experimental results (filled dots of

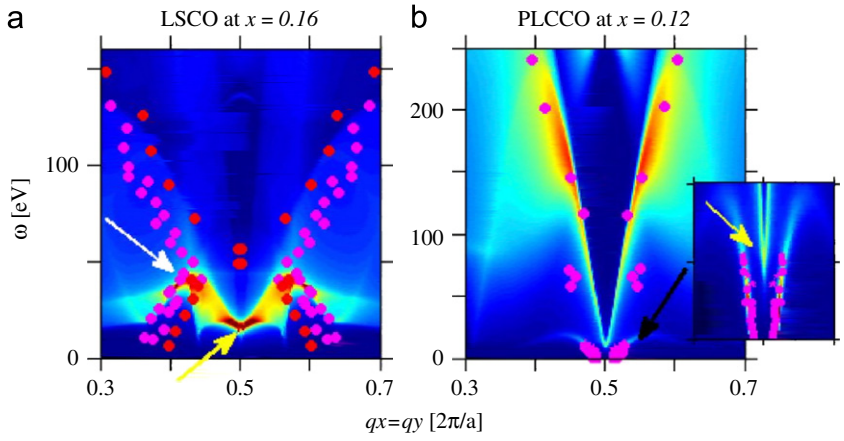

Fig. 5. (Color online) Computed magnetic excitation spectrum along the (π,π) direction in optimally doped LSCO (left) and PLCCO (right) discussed in the text is shown in the color plots. Filled symbols of various shapes are from neutron data in the literature [45]. The low energy region in PLCCO is shown in the inset on an expanded energy scale. (After Ref. [44].)

various shapes) in both LSCO and PLCCO [45]. In particular, the theoretical spectra yield striking differences between LSCO and PLCCO, including a smaller value of the resonance energy in PLCCO compared to LSCO, display the characteristic hour-glass shape and upward dispersion with momentum, and a 45° rotation of the peak intensity as the hourglass crosses the peak energy, all in accord with the neutron scattering data. A number of weaker features are also predicted theoretically, such as the second branch seen in the inset in PLCCO, and other weak branches in LSCO.

In summary, we have discussed how a comprehensive scheme for modeling various highly resolved spectroscopies of the cuprates can be obtained by adding appropriate self-energy corrections into the one-particle electron and hole Green's functions. The interplay of matrix element, crystal structure and electron correlations is shown to lead to surprising results in a number of problems of current interest involving ARPES, STS, optical and magnetic excitation spectra of electron and hole doped curpates [46–48]. Our modeling framework provides a fairly sophisticated baseline for ascertaining the extent to which standard pictures (LDA, beyond-LDA, various structural effects) are at play, and constitutes thus a reliable basis for identifying signatures of truly exotic features in the spectra.

Acknowledgments

This work is supported by the US Department of Energy, Office of Science, Basic Energy Sciences contract DE-FG02-07ER46352, and benefited from the allocation of supercomputer time at NERSC, and Northeastern University's Advanced Scientific Computation Center (ASCC).

References

[1] A. Bansil, M. Lindroos, Phys. Rev. Lett. 83 (1999) 5154;
A. Bansil, et al., New J. Phys. 7 (2005) 140.
[2] R.S. Markiewicz, A. Bansil, Phys. Rev. B 75 (2007) 020508.
[3] R.S. Markiewicz, S. Sahrakorpi, A. Bansil, Phys. Rev. B 76 (2007) 174514.
[4] R.S. Markiewicz, T. Das, S. Basak, A. Bansil, J. Electron Spectrosc. Relat. Phenom. 181 (2010) 23.
[5] T. Das, R.S. Markiewicz, A. Bansil, Phys. Rev. B 81 (2010) 174504.
[6] T. Das, R.S. Markiewicz, A. Bansil, Phys. Rev. B 81 (2010) 184515.
[7] R.S. Markiewicz, et al., Phys. Rev. B 72 (2005) 054519.
[8] A. Bansil, et al., Phys. Rev. B 60 (1999) 13396;
L. Schwartz, A. Bansil, Phys. Rev. B 10 (1974) 3261;
R. Prasad, A. Bansil, Phys. Rev. B 21 (1980) 496;
A. Bansil, Z. Naturforschung A 48 (1993) 165.
[9] S.N. Khanna, et al., Solid State Commun. 55 (1985) 223;
L. Huisman, et al., Phys. Rev. B 24 (1981) 1824.
[10] H. Lin, et al., Phys. Rev. Lett. 96 (2006) 097001.
[11] T. Dahm, et al., Nat. Phys. 5 (2009) 217.
[12] R.S. Markiewicz, A. Bansil, Phys. Rev. B 78 (2008) 134513.
[13] C. Kusko, et al., Phys. Rev. B 66 (2002) 140513.
[14] T. Das, R.S. Markiewicz, A. Bansil, Phys. Rev. Lett. 98 (2007) 197004.
[15] E.G. Moon, S. Sachdev, Phys. Rev. B 80 (2009) 035117.
[16] T. Das, R.S. Markiewicz, A. Bansil, Phys. Rev. B 77 (2008) 134516;
T. Das, R.S. Markiewicz, A. Bansil, Phys. Rev. B 77 (2008) 219904.
[17] S. Johnston, et al., arXiv:1007.3451, 2010.
[18] E. Schachinger, J.P. Carbotte, T. Timusk, Europhys. Lett. 86 (2009) 67003.
[19] F. Giustino, M.L. Cohen, S.G. Louie, Nature 452 (2008) 975.
[20] A. Macridin, et al., Phys. Rev. Lett. 99 (2007) 237001.
[21] D.S. Inosov, et al., Phys. Rev. Lett. 99 (2007) 237002;
D.S. Inosov, et al., Phys. Rev. B 77 (2008) 212504;
D.S. Inosov, et al., Phys. Rev. B 79 (2009) 139901(E).
[22] F. Ronning, et al., Phys. Rev. B 71 (2005) 094518.
[23] J. Graf, et al., Phys. Rev. Lett. 98 (2007) 067004.
[24] W. Meevasana, et al., Phys. Rev. B 75 (2007) 174506.
[25] B. Moritz, et al., New J. Phys. 11 (2009) 093020.
[26] P.W. Anderson, Science 316 (2007) 1705.
[27] T.A. Maier, D. Poilblanc, D.J. Scalapino, Phys. Rev. Lett. 100 (2008) 237001.
[28] S. Basak, et al., Phys. Rev. B 80 (2009) 214520.
[29] S. Sahrakorpi, et al., Phys. Rev. Lett. 95 (2005) 157601;
A. Bansil, et al., Phys. Rev. B 71 (2005) 012503;
M.C. Asensio, et al., Phys. Rev. B 67 (2003) 014519.
[30] C.M. Varma, Phys. Rev. B 61 (2000) R3804;
M.E. Simon, C.M. Varma, Phys. Rev. Lett. 89 (2002) 247003.
[31] A. Kaminski, et al., Nature 416 (2002) 610.
[32] V. Arpiainen, A. Bansil, M. Lindroos, Phys. Rev. Lett. 103 (2009) 067005.
[33] J.P. Castellan, et al., Phys. Rev. B 73 (2006) 174505;
P.A. Miles, et al., Physica (Amsterdam) 294C (1998) 275.
[34] S.V. Borisenko, et al., Nature 431, DOI: 10.1038/nature02931, 2004.
[35] J. Nieminen, et al., Phys. Rev. Lett. 102 (2009) 037001;
J. Nieminen, I. Suominen, R.S. Markiewicz, H. Lin, A. Bansil, Phys. Rev. B 80 (2009) 134509.
[36] K. McElroy, et al., Science 309 (2005) 1048.
[37] I. Martin, A.V. Balatsky, J. Zaanen, Phys. Rev. Lett. 88 (2002) 097003.
[38] P.W. Anderson, P.N. Ong, J. Phys. Chem. Solids 67 (2006) 1;
M. Randeria, et al., Phys. Rev. Lett. 95 (2005) 137001.
[39] T. Arima, Y. Tokura, S. Uchida, Phys. Rev. B 48 (1993) 6597;
S. Uchida, et al., Phys. Rev. B 43 (1991) 7942;
Y. Onose, et al., Phys. Rev. B 69 (2004) 024504.
[40] R.S. Markiewicz, A. Bansil, Phys. Rev. Lett. 96 (2006) 107005;
Y.W. Li, et al., Phys. Rev. B 78 (2008) 073104.
[41] J. Rossat-Mignod, et al., Physica C: Superconductivity 185–189 (1991) 86;
H.A. Mook, et al., Phys. Rev. Lett. 70 (1993) 3490;
H.F. Fong, et al., Phys. Rev. Lett. 75 (1995) 316.
[42] G. Yu, et al., Nat. Phys. 5 (2009) 873.
[43] P.W. Anderson, Phys. Rev. Lett. 96 (2006) 017001;
F. Krüger, et al., Phys. Rev. B 76 (2007) 094506;
J.-P. Ismer, I. Eremin, E. Rossi, D.K. Morr, Phys. Rev. Lett. 99 (2007) 047005;
I. Eremin, D.K. Morr, A.V. Chubukov, K.H. Bennemann, M.R. Norman, Phys. Rev. Lett. 96 (2005) 147001;
M. Vojta, T. Vojta, R.K. Kaul, Phys. Rev. Lett. 97 (2006) 097001.
[44] T. Das, R.S. Markiewicz, A. Bansil, unpublished.
[45] Experimental data are taken from following sources: LSCO (red dots) for $x=0.16$ from B. Vignolle, et al., Nature Phys. 3 (2007) 163; Magenta dots, LBCO ($x=0.12$) from J.M. Tranquada, et al., Nature 429 (2004) 534; PLCCO ($x=0.12$), square and star at low energy region from S.D Wilson, et al., Nature 442 (2006) 59; Circles at high energy from S.D Wilson, et al., Phys. Rev. Lett. 96 (2006) 157001.
[46] It will be interesting to examine effects of self-energy corrections in high-resolution Compton scattering [47] and positron-annihilation [48] spectra, which probe ground state momentum density of the electronic system.
[47] Y. Tanaka, et al., Phys. Rev. B 63 (2001) 045120;
S. Huotari, et al., Phys. Rev. B 62 (2000) 7956;
G. Stutz, et al., Phys. Rev. B 60 (1999) 7099.
[48] L.C. Smedskjaer, et al., Physica C 192 (1992) 259;
P.E. Mijnarends, et al., J. Phys. Condens. Matter 10 (1998) 10383.